Efficacy of synthesis conditions on functionalized carbon nanotube blended cellulose acetate membrane for desalination

Hyeon-gyu Choi[a], Sang Hyeon Yoon[a], Moon Son[a], Evrim Celik[b], Hosik Park[c,*], Heechul Choi[a,*]

[a]School of Environmental Science and Engineering, Gwangju Institute of Science and Technology (GIST), 123 Cheomdan-gwagiro, Buk-gu, Gwangju 500-712, Korea, Tel. +82 62 7152441; Fax: +82 62 7152434; email: hcchoi@gist.ac.kr (H.-g. Choi)
[b]Faculty of Engineering, Department of Environmental Engineering, Suleyman Demirel University, 32260, Isparta, Turkey
[c]Center for Membranes, Advanced Materials Division, Korea Research Institute of Chemical Technology (KRICT), Daejeon 305-600, Republic of Korea, Tel. +82 42 8607510; Fax: +82 42 8607533; email: hspark@krict.re.kr (H. Park)

ABSTRACT

Cellulose acetate membrane has been applied to reverse osmosis for desalination due to chlorine tolerance and biofouling resistance. Since it requires optimized synthesis condition for application, we investigated the effect of different conditions on membrane performances. It was found that polymer concentration, solvent ratio, and evaporation time were critical to determine membrane selectivity and permeability. Based on the study, optimized conditions were obtained, which were 14 wt% of polymer concentration, 1:2.9 of ratio of 1,4-dioxane to acetone, and 30 s of evaporation time. Further, functionalized multi-walled carbon nanotubes (MWCNTs) were applied to the optimized bare membrane in order to enhance the performances. The composite membranes were characterized by fourier transform infrared spectroscopy, scanning electron microscopy, and contact angle measurement. It was found that the MWCNTs influenced the morphology and surface chemistry of the membrane. This study could contribute to develop a commercial composite RO membrane with nanomaterial for desalination application.

Keywords: Reverse osmosis; Cellulose acetate; Phase inversion; Fabrication optimization; Carbon nanotube; Functionalization

1. Introduction

Recently, it has been a critical issue to obtain clean and enough drinking water all around the world. Since surface water from rivers or lakes occupies the only 0.01% of the whole water resource on the earth, it cannot sufficiently cover global water demand.

Oceans, occupying 97% of the earth water, can be a fundamental candidate to solve global water scarcity [1]. Huge technical efforts in desalination have been devoted for stable drinking water supply because desalination generates drinking water from ultimate water source of the sea [2]. Distillation, electrodialysis, and reverse osmosis are widely utilized in desalination technology. Recently, reverse osmosis has been

*Corresponding authors.

commonly applied in desalination market whereas distillation had been applied in the last decades. Reverse osmosis membrane fabrication is one of the core element technologies in desalination process. There are two types of RO membranes: cellulose acetate (CA) asymmetric membrane and thin-film composite (TFC) membrane. Currently, TFC membrane is widely used in RO process due to its low energy consumption and good permselectivity. CA membrane has been partially used due to its excellent tolerance for chlorine ion and micro-organism. However, CA membrane has technical limitation which is relatively low water flux [3].

Membrane hydrophilicity is an important factor to enhance water flux and membrane fouling resistance [4]. Several methods to increase hydrophilicity have been conducted such as surface graft polymerization, chemical grafting, and radiation grafting [5]. As nanotechnology has been actively applied to environmental field, organic–inorganic hybrid membrane has been studied recently [6]. In particular, nanosize inorganic material blended membrane has received much interest because of its significantly enhanced hydrophilicity and anti-fouling. Alumina, titania, and carbon nanotube (CNT) have been mostly applied [7–9].

CNT is one of the remarkable nanomaterials applied to organic–inorganic hybrid membrane due to its strong chemical property, high strength and stiffness, high aspect ratio in combination with low blending amount, which can be an effective additive for polymer composites [10]. However, extremely hydrophobic surface of CNTs interrupts water passage through membrane. Appropriate functionalization method is necessary to allow CNTs hydrophilic property via attaching functional groups such as carboxyl ($-COOH$), amine ($-NH_2$), and hydroxyl ($-OH$) on the CNTs surface [11].

This study suggests multi-walled carbon nanotubes (MWCNTs)/CA composite membrane for desalination application. The main objectives of this study can be (1) to synthesize CA membrane by optimizing synthesis conditions (polymer concentration, solvent composition, evaporation time), (2) to synthesize MWCNTs blended CA membrane based on the optimized conditions, (3) to investigate an effect of the MWCNTs on membrane characteristics and performances for desalination application.

2. Experimental

2.1. Materials and chemicals

CA (CA, Mw ~30,000 g/mol, acetyl content of 39.8 wt%), acetone (>99.5%), and methanol (>99.8%),

sulfuric acid (H_2SO_4, >98%), nitric acid (HNO_3, >70%), sodium chloride (NaCl) were obtained by Sigma–Aldrich. 1,4-dioxane was supplied by Arcos company. Lactic acid was purchased from Fluka. Sodium sulfate (Na_2SO_4) was purchased from oriental chemical industry in Korea. The multi-walled carbon nanotube (MWCNTs, >98%) with 10–40 nm in outer diameter were obtained from Hanwha Nanotech. Co. Ltd (Korea). PET nonwoven fabric was supplied by AMFOR incorporation. All of the aqueous solutions for the experiments were prepared using deionized (DI) water from a water purification system (Synergy, Millipore, USA) which has a resistivity of 18.2 mΩ cm.

2.2. Carbon nanotube functionalization and membrane fabrication

The MWCNTs were functionalized followed by acid treatment. Raw MWCNTs were soaked in a mixture of nitric acid and sulfuric acid (3:1, v/v) to remove impurities and increase dispersion in solvents [12]. The mixture of the acids and MWCNTs was refluxed at 100°C for 3 h. Next, it was rinsed with DI water to reach to pH 7.0 ± 0.2. The rinsed MWCNTs were dried at room temperature for 24 h. The dried MWCNTs were ultrasonicated in the same volume of HNO_3: H_2SO_4 mixture at 70°C for 9 h. Finally, the MWCNTs were washed with DI water until pH reached to 7.0 ± 0.2. The washed MWCNTs were dried in an oven at 100°C overnight and stored in room temperature.

To optimize synthesis conditions, CA polymer bare membranes were fabricated via classical phase inversion method. The CA polymer was added into a solvent mixture of 1,4-dioxane and acetone at room temperature and stirred for 12 h for complete dissolving. Methanol and lactic acid were next added into the polymer solution, and the solution was casted using manually casting knife with 200 μm thickness on PET fabric. After exposure to the air to allow the casted polymer film evaporated, the casted polymer was dipped in DI water overnight. Next, the membrane was washed with DI water and stored in DI water. To investigate the effects of synthesis conditions on membrane characteristics and performances, different conditions were applied—polymer concentration, solvent ratio, and evaporation time.

MWCNTs/CA (CNT/CA) membranes were fabricated by the same phase inversion method with the CA bare membrane. Functionalized MWCNTs were ultrasonicated in the solvent for good dispersion. After dispersing MWCNTs, the CNT/CA composite membranes were prepared following optimized conditions drawn by bare membrane test.

2.3. MWCNTs and membrane characterization

The raw and functionalized MWCNTs morphologies were characterized using transmission electron microscopy (TEM, JEM-2100, JEOL, Japan). The functional groups of the MWCNTs and the synthesized membranes were analyzed using fourier transform infrared spectroscopy (FTIR, Nicolet iS10, Thermo Scientific, USA). Specific surface area and porosities of the MWCNTs were measured using surface area and porosity analyzer (ASAP 2020, micromeritics, USA). The membranes morphologies were characterized using scanning electron microscopy (SEM, S-4700, Hitachi, Japan). The hydrophilicity of the membrane surface was evaluated through the dynamic sessile drop method, using a contact angle goniometer (Model 100, Rame-Hart, USA). A minimum of seven contact angles were averaged to ensure reliable values.

2.4. Lab-scale RO performance test of the CNT/CA membrane

Lab-scale RO filtration setup was utilized to evaluate the CNT/CA membranes performances. Temperature was maintained at $20°C ± 0.5$. Effective membrane area in RO mode was 30 cm². Operation pressure of a test unit was applied to 30 bars and a circulation cross flow rate was applied to 600 mL/min. A pure water flux was calculated using the following equation:

$$J_w = \frac{V}{At} \tag{1}$$

where J_w is the water flux (L/m² h), V is the volume of water permeated through the membrane (L), A is the effective membrane area (m²), and t is the time (h). NaCl and Na_2SO_4 rejections of the membranes in RO mode were calculated using the following equation:

$$R = \left(1 - \frac{C_p}{C_f}\right) \times 100 \tag{2}$$

where R is the salt ion rejection (%), C_f and C_p are the concentrations of the feed solution and permeate solution, respectively. The concentrations of feed and permeate solutions were measured with electrical conductivity by using pH/conductivity meter (CPC-401, Elmetron, Poland). About 5,000 ppm NaCl and 200 ppm Na_2SO_4 were added in the feed solutions, respectively. All the lab-scale RO tests were conducted after an 18 h stabilization period for compaction of the membranes.

3. Results and discussion

3.1. Cellulose acetate bare membrane

3.1.1. Effect of polymer concentration

Different CA polymer concentrations were applied from 13 to 18 wt% in the casting solution to investigate the effect of polymer concentration on membrane characteristics and performances. All the membranes were synthesized by same preparation process with fixed solvent ratio (1,4-dioxane:acetone = 2.9:1, volume ratio) and 30 s of the evaporation time, followed by immersion of the membrane in a coagulation bath with DI water.

Fig. 1 shows the pure water fluxes of the CA bare membranes with the different polymer concentration. The pure water flux of the 18 wt% CA bare membrane was minimized to 43.6 L/m² h and the second lowest flux was observed when 14 wt% CA bare membrane as 63.3 L/m² h. The 13 wt% CA bare membrane showed the highest pure water flux as 95.3 L/m² h. As increasing of polymer concentration, the pure water flux was gradually decreased as CA polymer concentration was increased, except 14 wt% CA membrane.

The solute diffusion in membrane formation is defined that permeates dissolve in the membrane and then diffuse through the membrane down a concentration gradient. It drives permeates transported in the membrane using the difference in the solubility of materials in the membrane and difference in the diffuse rates of materials in the membrane. It is known that the driving force of pressure and concentration with flow are important factors to explain the solute diffusion. Increasing polymer concentration leads to the preparation of thinner and denser membrane [13]. Higher polymer concentrations induce to chain entanglement so that the membrane pore structure became dense and small. This structure lead to high pressure resistance, therefore, the pure water flux is decreased.

In the bottom of Fig. 1, the 14 wt% CA bare membrane showed the highest selectivity—Na_2SO_4 rejection: 83.6% and NaCl rejection: 45.2%, whereas the 13 wt% CA bare membrane showed the lowest rejections—Na_2SO_4 rejection: 55.2% and NaCl rejection: 16.8%, respectively. Excepting the 13 wt% CA bare membrane, the rejections became gradually reduced as polymer concentration was increased. As polymer concentration is increased, it required longer time to start liquid–liquid phase separation due to its high viscosity, hence it is difficult to complete a phase inversion process. In addition, delayed liquid–liquid phase separation leads to form a metastable membrane [14], which cannot induce well-developed dense
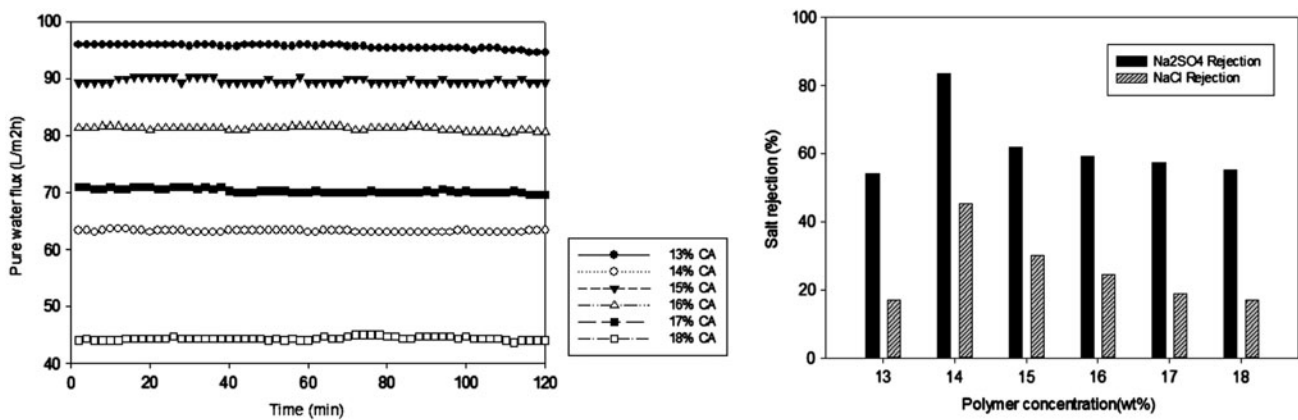
Fig. 1. Pure water flux (left) and salt ion rejection (right) of the CA bare membrane with different polymer concentration.

layer on the membrane surface resulting in poor salt ion selectivity of the membranes.

SEM images of the membranes with different polymer concentration are shown in Fig. 2. All the membranes exhibited the asymmetric structure with finger-like pores on the bottom and dense layer on the top surface. As polymer concentration was increased, sub-layer of the membrane became denser and it indicates that the membrane porosity was decreased. In addition, thinner membrane was synthesized by increasing polymer concentration. Generally, the membrane porosity governs pure water flux because dense polymer structure in membrane matrix directly interrupts water passage. Similarly, the membrane thickness is also highly related to water molecule transport through the membrane. In this study, the membranes with large porosity showed high pure water flux.

Despite the thinnest structure, the 18 wt% CA bare membrane with the least porosity showed the lowest water flux. It implies that dense structure in membrane matrix is more critical to determine the water flux rather than membrane thickness. Further, the 14 wt% CA bare membrane has well-developed dense active layer on the top of the membrane, which induced unexpectedly low pure water flux.

Based on the membrane performances, the 14 wt% CA bare membrane was determined as an optimum polymer concentration condition due to its highest selectivity.
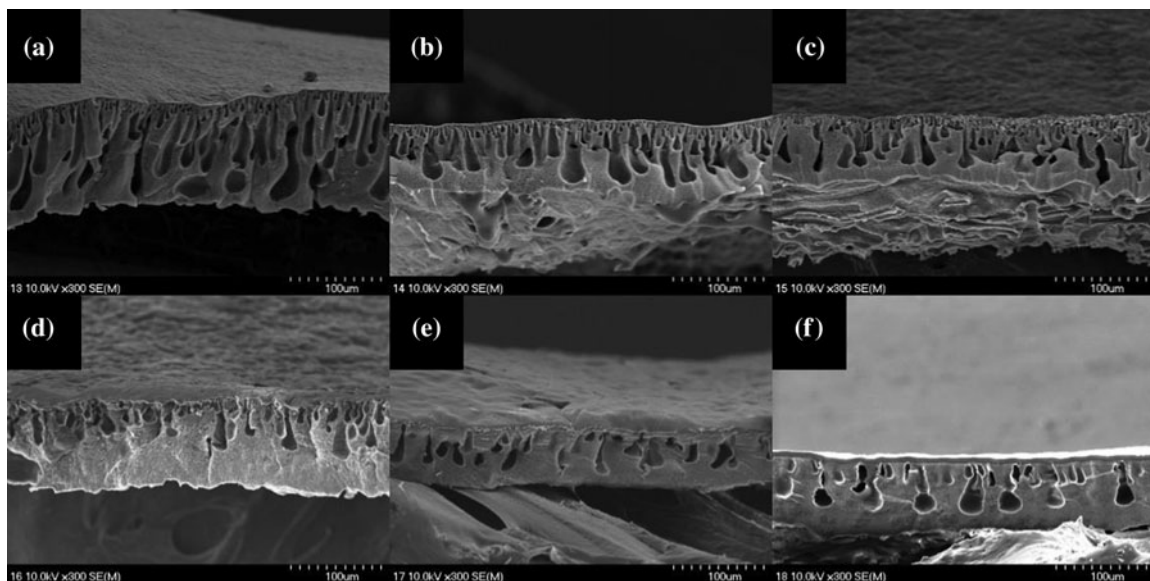

Fig. 2. SEM cross-sectional images of the CA bare membrane with different polymer concentration: (a) 13 wt%, (b) 14 wt%, (c) 15 wt%, (d) 16 wt%, (e) 17 wt%, and (f) 18 wt%.

3.1.2. Effect of solvent ratio

Solvent ratios also affect a formation of membrane morphology during phase inversion. Different volume ratios of 1,4-dioxane and acetone mixture were applied to the CA bare membrane fabrication—(14_1) 1,4-dioxane only, (14_2) 1,4-dioxane:acetone = 2.9:1, (14_3) 1,4-dioxane:acetone=1:1, (14_4) 1,4-dioxane:acetone = 1:2.9, (14_5) acetone only (Table 1). The evaporation time was controlled at 30 s before immersion step of the membrane in a coagulation bath.

Fig. 3 shows the pure water flux changes of the CA bare membranes based on the solvent composition. 14_5 membrane with the largest amount of acetone had the lowest water flux as 10 L/m² h, and the second lowest flux showed in 14_4 membrane as 42.5 L/m² h. The pure water flux was maximized when 1,4-dioxane itself was applied in 14_1 membrane as 70.5 L/m² h. It indicates that the pure water flux was reduced as acetone ratio was increased in the solvent mixture. It was reported that the presence of higher quantity of acetone in the polymer solution forms less porous and dense structure on the surface [15].

The salt ion rejection results indicate that 14_1 membrane showed the lowest salt rejection—the

rejections of Na_2SO_4 and NaCl were 66.1 and 30.4%. The solvent of 1,4-dioxane leads to the highest pure water flux but salt rejection for the casted membrane from this solvent is poor. 14_5 membrane with only acetone has rejections of Na_2SO_4 and NaCl were 86.2, 51.7%, which were the highest salt rejections. It is interesting that 14_4 membrane has second highest salt rejection—the rejection of Na_2SO_4 was 86.1%, and the rejection of NaCl was 50.6%, which was similar with 14_5 membrane. Considering the water flux and salt rejection, it suggested that the optimum solvent composition membrane is 14_4 membrane which consist of 1,4-dioxane:acetone = 1:2.9 due to its relatively high flux and salt rejection.

The membrane morphology change with different solvent composition was observed via SEM images (Fig. 4). As increased acetone composition, the membrane structure became dense, but the porosity of top layer was reduced. High acetone composition led to decrease in pure water flux due to the dense and lower porosity of top layer, but this structure can be attributed to enhance membrane selectivity, which was caused by slower exchange rate between acetone and DI water during the phase inversion [16]. Therefore, 14_5 membrane had the densest structure on the top layer due to high acetone ratio.

3.1.3. Effect of evaporation time

During evaporation step, solvent goes out of the casted membrane surface, thus increasing polymer concentration of the top surface layer in the membrane. It induces denser surface layer membranes. The evaporation time was varied from 15 to 60 s to investigate an evaporation effect.

Table 1
Polymer solution with different solvent ratio

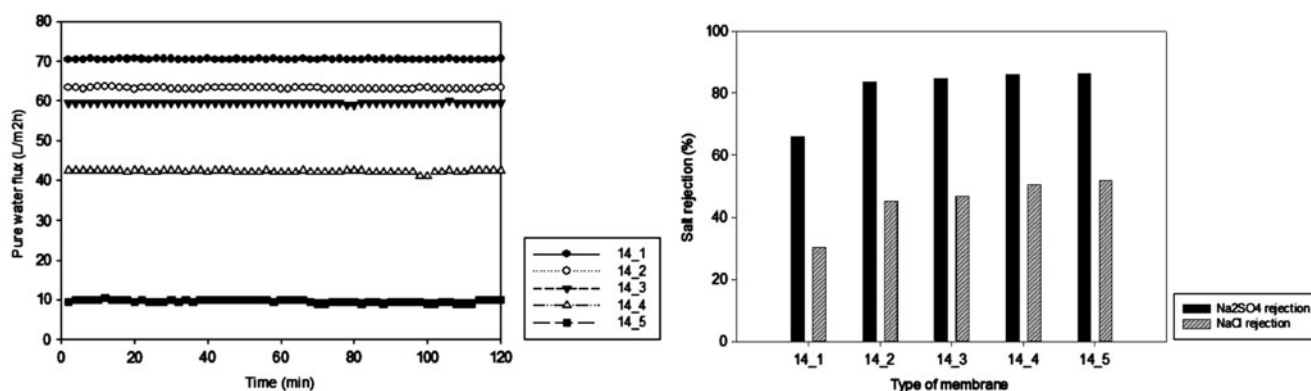| Membrane	Solvent volume ratio (1,4-dioxane:acetone)
14_1	1,4-dioxane only
14_2	2.9:1
14_3	1:1
14_4	1:2.9
14_5	Acetone only

Fig. 3. Pure water flux (left) and salt ion rejection (right) of the CA bare membrane with different solvent ratio. (14_1) 1,4-dioxane only, (14_2) 1,4-dioxane:acetone = 2.9 : 1, (14_3) 1,4-dioxane:acetone = 1 : 1, (14_4) 1,4-dioxane:acetone = 1 : 2.9, (14_5) acetone only.
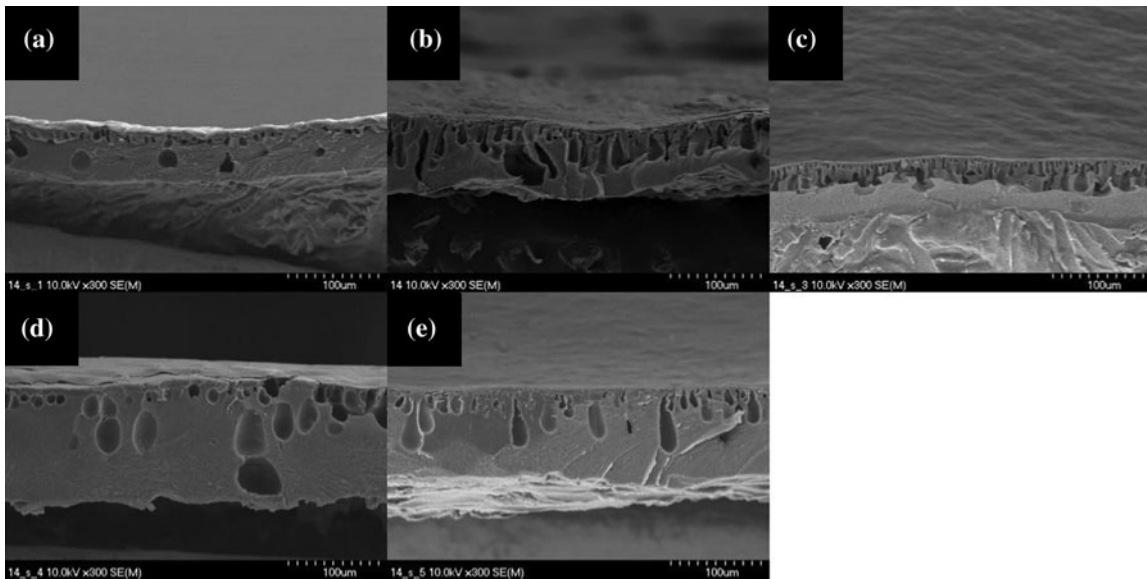
Fig. 4. SEM cross-sectional images of the CA bare membrane with different solvent ratio: (a) 14_1 (1,4-dioxane only), (b) 14_2 (1,4-dioxane:acetone = 2.9 : 1), (c) 14_3 (1,4-dioxane:acetone = 1 : 1), (d) 14_4 (1,4-dioxane : acetone = 1:2.9), and (e) 14_5 (acetone only).

The effect of evaporation time on membrane pure water flux is illustrated in Fig. 5. The water flux change trend demonstrated that the CA bare membrane with 30 s evaporation had the lowest pure water flux as 42.5 L/m^2 h, but the membrane with 15 and 60 s evaporations had relatively higher pure water fluxes as 95 and 93.5 L/m^2 h. Longer evaporation time results in bigger and more uniform pores on the surface whereas shorter evaporation time results in smaller and less uniform pores on the surface. However, too long evaporation time does not improve the membrane selectivity, which leads to less than critical size, pores on prolonged evaporation [17].

The Na$_2$SO$_4$ and NaCl rejection of 15 s evaporation time membrane were 57.6 and 28.1%. The membrane with 45 s evaporation time had 60.3% of Na$_2$SO$_4$ rejections and 33.1% of NaCl rejection. The lowest salt rejection showed the membrane with 60 s evaporation time whose rejections of Na$_2$SO$_4$ and NaCl are 53.5 and 19.9%. The membrane with 30 s evaporation time had the highest salt rejection—the rejections of Na$_2$SO$_4$ and NaCl are 86.1 and 50.6%.

In Fig. 6, cross-sectional membrane morphologies showed that the increased evaporation time up to 30 s led to denser and less porous top layer of the membrane. However, the porosity of top layer was increased
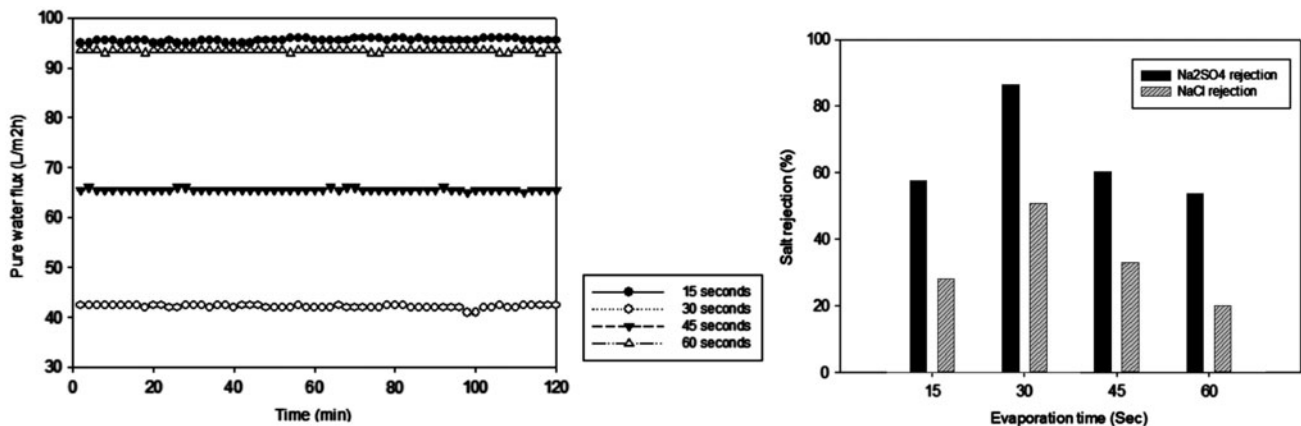

Fig. 5. Pure water flux (left) and salt ion rejection (right) of the CA bare membrane with different evaporation time.
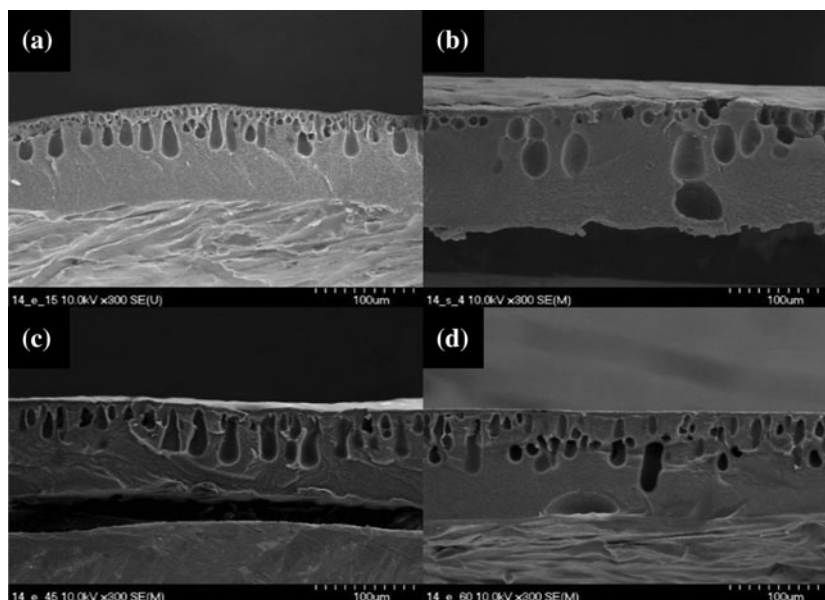
Fig. 6. SEM cross-sectional images of the CA bare membrane with different evaporation time: (a) 15 s, (b) 30 s, (c) 45 s, and (d) 60 s.

when evaporation time exceed 30 s. It is contributed that the pure water flux was the lowest at 30 s of evaporation time, but the pure water flux was increased by longer or shorter than 30 s of evaporation time.

It is pointed out that the evaporation time is critically an important step regarding the membrane selectivity. An appropriate evaporation time is necessary to promise high salt ion rejection [18]. It suggested that the optimum evaporation time is 30 s in this study.

3.2. MWCNTs blended Cellulose Acetate Membrane (CNT/CA Membrane)

3.2.1. MWCNTs Characterization

The TEM images of the raw MWCNTs and functionalized MWCNTs are shown in Fig. S1. As shown in Fig. S1 (a) and (b), TEM images indicated that raw MWCNTs tend to manufacture aggregates because the length of raw MWCNTs is relatively long, while the MWCNTs were highly dispersed after functionalization. The MWCNTs bundles were shortened through acid treatment [19]. As shown in Fig. S1 (c) and (d), the TEM images show that the end-tips of the raw MWCNTs were closed, but the end-tips of the functionalized MWCNTs were opened.

Fig. S2 shows FTIR spectra of raw/functionalized MWCNTs and the CNT/CA membranes. After functionalization treatment, the peaks are emerged at 1,500–1,600, and 3,300–3,500 cm^{-1}. The peak of 1,500–1,600 cm^{-1} can be associated with COOH groups. The peak of 3,300–3,500 cm^{-1} corresponded to hydroxyl bond (O–H) in the COOH groups [20]. It can be attributed to the formation of carboxyl functional group onto the MWCNTs surface via functionalization.

Functionalized MWCNTs blended CA membranes are similar peaks with bare CA membrane. Additional functional group spectra were observed in CNT/CA membranes with the peaks 1,730, 1,340, and 1,300 cm^{-1} which are corresponded to C=O, COO^{-}, and COOH groups. Moreover, it described that the CNT/CA membranes might form via hydrogen bonding interactions between the carboxyl groups of CA and the hydroxyl groups of functionalized MWCNTs [21].

3.2.2. CNT/CA membrane characterization

The membrane hydrophilicity was evaluated by water contact angle measurement (Fig. S3). The contact angles of the CNT/CA membranes gradually decreased as the MWCNTs concentration was increased in the membrane. It indicated the hydrophilicity of the membrane was improved by blending MWCNTs. The functionalized MWCNTs moved spontaneously to the interface between membrane and water to reduce the interface energy during phase inversion process [22,23].

SEM images of surface and cross-sectional structures of the membranes were shown in Fig. 7. By blending MWCNTs, the color of the top surface became darker. It represents that more MWCNTs were

located on the top of the membrane matrix. The 0.5 and 1% CNT/CA membranes showed significant morphology change. The large numbers of macropores were observed in sub-layer of two membranes. The fast exchange of solvent and nonsolvent in the phase inversion process occurred due to the hydrophilic MWCNTs [24]. Immediate demixing process resulted in the formation of macrovoids and greater pores on the membrane [25].

On the other hand, when 2% MWCNTs was applied, the macropore size sub-layer was reduced. This result may be explained by the viscosity increase in the MWCNTs polymer solution, resulting from the delayed exchange of solvent and nonsolvent in phase inversion [26]. When a membrane is immersed into the coagulation bath containing nonsolvent such as DI water, two types of demixing processes occurs: formation of aggregates and liquid–liquid phase separation. Formation of aggregates begins because solvent and the nonsolvent are also miscible in top surface of membrane and sub-layer. Liquid–liquid phase separation takes place due to the low miscibility between CA polymer and the nonsolvent, which leads to the formation of nucleuses of polymer. However, when the viscosity of solution is relatively high, it required time to start liquid–liquid phase separation due to its high viscosity. Hence, the longer time need to finish demixing process when MWCNTs content is high. It leads to thinner and denser membrane [13].

3.2.3. CNT/CA membrane performance test

Generally, the water permeation is determined by hydrophilicity and porosity of the membrane. The pure water flux change trend was similar with the
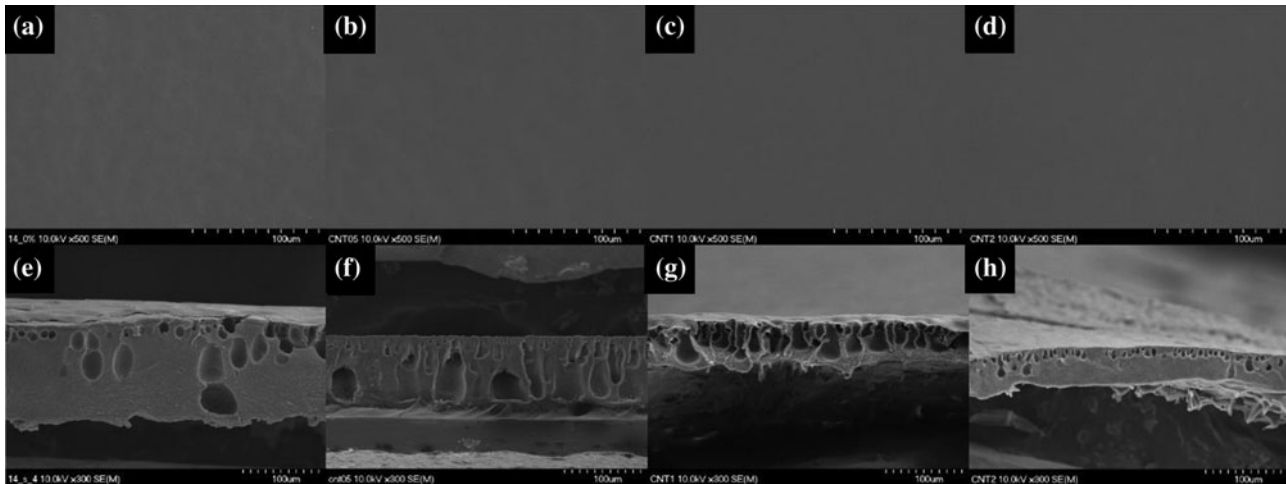

Fig. 7. SEM images of the surface (top) and cross-sectional (bottom) morphologies of the CNT/CA membranes: (a,e) the CA bare membrane, (b,f) 0.5% CNT/CA membrane, (c,g) 1% CNT/CA membrane, and (d,h) 2% CNT/CA membrane.
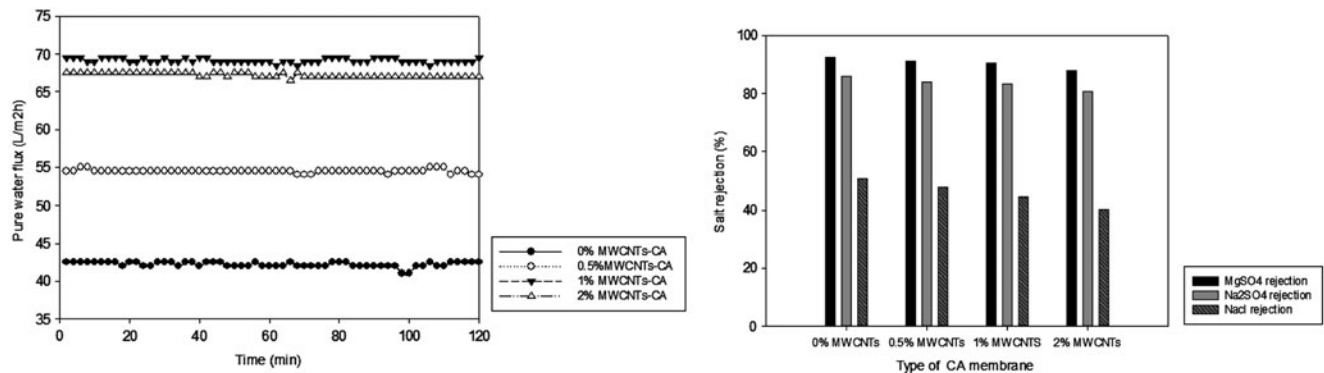

Fig. 8. Pure water flux (left) and salt ion rejection (right) of the CNT/CA membranes.

hydrophilicity change of the CNT/CA membrane in Fig. 8. The highest water flux (69.5 L/m^2 h) was observed in the 1% CNT/CA membrane. The 2% CNT/CA membrane with the most hydrophilicity showed slightly lower water flux (67 L/m^2 h) than 1% CNT/CA membrane. The 1% CNT/CA membrane improved 63% of pure water flux enhancement compared with the CA bare membrane.

The salt ion rejections of the membranes in descending order were followed as R(MgSO$_4$) > R(Na$_2$SO$_4$) > R(NaCl) due to Donnan exclusion [27]. A membrane has an electrical charge by adsorb ions of solutions or the blended MWCNTs on the membrane, particularly, surface of membrane [28]. Donnan exclusion is dependent on the surface charge of membrane, the ionic strength, and the valence ions [29]. Ions with the same charged membrane is called as co-ions, and the opposite charged ions are called as counter-ions. Co-ions are repelled, but counter-ions are attracted by membrane due to their electric property. It leads a chemical potential difference at the interface between membrane and solution, which is called as Donnan potential. To achieve equilibrium in this potential, co-ions are repelled, particularly bivalent co-ions, but counter-ions are attracted. The CNT/CA membranes are negatively charged, the higher rejection was for Na$_2$SO$_4$ and lower rejection was for NaCl. Comparing the rejections of MgSO$_4$ and Na$_2$SO$_4$, the rejection of MgSO$_4$ is higher than Na$_2$SO$_4$, it is because that the order of rejection of ions is as shown for cations Mg^{2+} > Na$^+$.

Moreover, the salt rejection was dependent on the MWCNTs contents. The salt rejection for bare membrane is the highest—MgSO$_4$, Na$_2$SO$_4$, and NaCl rejection were 92.5, 86.1, and 50.6%, respectively. By blending the MWCNTs, the salt rejection was reduced —(a) the 0.5% CNT/CA membrane: 91.2% of MgSO$_4$ rejection, 84.1% of Na$_2$SO$_4$ rejection, and 47.8% of NaCl rejection, (b) the 1% CNT/CA membrane: 90.6% of MgSO$_4$ rejection, 83.3% of Na$_2$SO$_4$ rejection, and 44.6% of NaCl rejection, (c) the 2% CNT/CA membrane: 87.8% of MgSO$_4$ rejection, 80.7% of Na$_2$SO$_4$ rejection, and 40.2% of NaCl rejection. It was reported that increasing concentration of functionalized MWCNTs leads to form macrovoids between polymer segments on the membrane surface [30,31]. According to those results, CA membrane with 1% MWCNTs was superior to the other membrane due to their high pure water flux and good salt rejection.

4. Conclusions

The fabrication and MWCNT blending effect of the CA membrane in RO were investigated, with several conclusions subsequently drawn. These conclusions include the following.

(1) The critical fabrication factors of CA membrane in RO were obtained, which were polymer concentration, solvent ratio, and evaporation time. Those influenced membrane morphology resulting in changing membrane performances in RO mode.
(2) Selected fabrication conditions were determined as—14 wt% of polymer concentration, 1:2.9 of ratio of 1,4-dioxane to acetone, and 30 s of evaporation time.
(3) The functionalized MWCNTs were blended to the optimized CA bare membrane. The membrane showed enhanced permeability and little reduced selectivity due to changes of morphology and surface chemistry.
(4) This MWCNT-CA membrane has a great potential to apply polymeric RO membrane having improved performances, however, its fabrication procedure might be optimized. This study could contribute nanomaterial blended polymeric RO membrane development as an initial trigger.

Supplementary material

The supplementary material for this paper is available online at http://dx.doi.10.1080/19443994.2015.1025582.

References

[1] T. Oki, S. Kanae, Global hydrological cycles and world water resources, Science 313 (2006) 1068–1072.
[2] L. García-Rodríguez, Renewable energy applications in desalination: State of the art, Sol. Energy 75 (2003) 381–393.
[3] H.B. Park, B.D. Freeman, Z.-B. Zhang, M. Sankir, J.E. McGrath, Highly chlorine-tolerant polymers for desalination, Angew. Chem. Int. Ed. 47 (2008) 6019–6024.
[4] Y.-Q. Wang, Y.-L. Su, Q. Sun, X.-L. Ma, Z.-Y. Jiang, Generation of anti-biofouling ultrafiltration membrane surface by blending novel branched amphiphilic polymers with polyethersulfone, J. Membr. Sci. 286 (2006) 228–236.

[5] Q. Shi, Y. Su, S. Zhu, C. Li, Y. Zhao, Z. Jiang, A facile method for synthesis of pegylated polyethersulfone and its application in fabrication of antifouling ultrafiltration membrane, J. Membr. Sci. 303 (2007) 204–212.

[6] R. Abedini, S.M. Mousavi, R. Aminzadeh, A novel cellulose acetate (CA) membrane using TiO₂ nanoparticles: Preparation, characterization and permeation study, Desalination 277 (2011) 40–45.

[7] L. Yan, Y.S. Li, C.B. Xiang, Preparation of poly(vinylidene fluoride)(pvdf) ultrafiltration membrane modified by nano-sized alumina (Al₂O₃) and its antifouling research, Polymer 46 (2005) 7701–7706.

[8] J.-H. Choi, J. Jegal, W.-N. Kim, Fabrication and characterization of multi-walled carbon nanotubes/polymer blend membranes, J. Membr. Sci. 284 (2006) 406–415.

[9] J.-F. Li, Z.-L. Xu, H. Yang, L.-Y. Yu, M. Liu, Effect of TiO₂ nanoparticles on the surface morphology and performance of microporous PES membrane, Appl. Surf. Sci. 255 (2009) 4725–4732.

[10] F.H. Gojny, M.H.G. Wichmann, U. Köpke, B. Fiedler, K. Schulte, Carbon nanotube-reinforced epoxy-composites: Enhanced stiffness and fracture toughness at low nanotube content, Compos. Sci. Technol. 64 (2004) 2363–2371.

[11] J.N. Coleman, A.B. Dalton, S. Curran, A. Rubio, A.P. Davey, A. Drury, B. McCarthy, B. Lahr, P.M. Ajayan, S. Roth, R.C. Barklie, W.J. Blau, Phase separation of carbon nanotubes and turbostratic graphite using a functional organic polymer, Adv. Mater. 12 (2000) 213–216.

[12] R. Sepahvand, M. Adeli, B. Astinchap, R. Kabiri, New nanocomposites containing metal nanoparticles, carbon nanotube and polymer, J. Nanopart. Res. 10 (2008) 1309–1318.

[13] C.C. Pereira, R. Nobrega, C.P. Borges, Membrane formation with presence of Lewis acid–base complexes in polymer solution, J. Appl. Polym. Sci. 83 (2002) 2022–2034.

[14] C.A. Smolders, A.J. Reuvers, R.M. Boom, I.M. Wienk, Microstructures in phase-inversion membranes. Part 1. Formation of macrovoids, J. Membr. Sci. 73 (1992) 259–275.

[15] A.D. Sabde, M.K. Trivedi, V. Ramachandhran, M.S. Hanra, B.M. Misra, Casting and characterization of cellulose acetate butyrate based UF membranes, Desalination 114 (1997) 223–232.

[16] M.L. Yeow, Y.T. Liu, K. Li, Morphological study of poly(vinylidene fluoride) asymmetric membranes: Effects of the solvent, additive, and dope temperature, J. Appl. Polym. Sci. 92 (2004) 1782–1789.

[17] R. Pilon, B. Kunst, S. Sourirajan, Studies on the development of improved reverse osmosis membranes from cellulose acetate–acetone–formamide casting solutions, J. Appl. Polym. Sci. 15 (1971) 1317–1334.

[18] N. Maximous, G. Nakhla, W. Wan, K. Wong, Preparation, characterization and performance of Al₂O₃/PES membrane for wastewater filtration, J. Membr. Sci. 341 (2009) 67–75.

[19] M. Vossoughi, S. Gojgini, A. Kazemi, I. Alemzadeh, Conjugation of amphotericin B to carbon nanotubes via amide-functionalization for drug delivery applications, Eng. Lett. 17 (2009) EL_17_4_12.

[20] S. Yang, J. Li, D. Shao, J. Hu, X. Wang, Adsorption of Ni(II) on oxidized multi-walled carbon nanotubes: Effect of contact time, pH, foreign ions and PAA, J. Hazard. Mater. 166 (2009) 109–116.

[21] M. Li, I.-H. Kim, Y.G. Jeong, Cellulose acetate/multi-walled carbon nanotube nanocomposites with improved mechanical, thermal, and electrical properties, J. Appl. Polym. Sci. 118 (2010) 2475–2481.

[22] M.C. Paiva, B. Zhou, K.A.S. Fernando, Y. Lin, J.M. Kennedy, Y.P. Sun, Mechanical and morphological characterization of polymer–carbon nanocomposites from functionalized carbon nanotubes, Carbon 42 (2004) 2849–2854.

[23] L. Dumée, K. Sears, J.R. Schütz, N. Finn, M. Duke, S. Gray, Carbon nanotube based composite membranes for water desalination by membrane distillation, Desalin. Water Treat. 17 (2010) 72–79.

[24] J.-F. Blanco, J. Sublet, Q.T. Nguyen, P. Schaetzel, Formation and morphology studies of different polysulfones-based membranes made by wet phase inversion process, J. Membr. Sci. 283 (2006) 27–37.

[25] E. Saljoughi, M. Sadrzadeh, T. Mohammadi, Effect of preparation variables on morphology and pure water permeation flux through asymmetric cellulose acetate membranes, J. Membr. Sci. 326 (2009) 627–634.

[26] O. Matarredona, H. Rhoads, Z. Li, J.H. Harwell, L. Balzano, D.E. Resasco, Dispersion of single-walled carbon nanotubes in aqueous solutions of the anionic surfactant NaDDBS, J. Phys. Chem. B 107 (2003) 13357–13367.

[27] J. Schaep, C. Vandecasteele, Evaluating the charge of nanofiltration membranes, J. Membr. Sci. 188 (2001) 129–136.

[28] M. Elimelech, W.H. Chen, J.J. Waypa, Measuring the zeta (electrokinetic) potential of reverse osmosis membranes by a streaming potential analyzer, Desalination 95 (1994) 269–286.

[29] M. Nilsson, G. Trägårdh, K. Östergren, The influence of pH, salt and temperature on nanofiltration performance, J. Membr. Sci. 312 (2008) 97–106.

[30] H.M. Yu, C. Ziegler, M. Oszcipok, M. Zobel, C. Hebling, Hydrophilicity and hydrophobicity study of catalyst layers in proton exchange membrane fuel cells, Electrochim. Acta 51 (2006) 1199–1207.

[31] J. Kim, B. Van der Bruggen, The use of nanoparticles in polymeric and ceramic membrane structures: Review of manufacturing procedures and performance improvement for water treatment, Environ. Pollut. 158 (2010) 2335–2349.